ADVANCES IN ATMOSPHERIC SCIENCES, VOL. 29, NO. 5, 2012, 1078–1088

Relationships between the Limit of Predictability and Initial Error in the Uncoupled and Coupled Lorenz Models

DING Ruiqiang* (丁瑞强) and LI Jianping (李建平)

State Key Laboratory of Numerical Modeling for Atmospheric Sciences and Geophysical Fluid Dynamics, Institute of Atmospheric Physics, Chinese Academy of Sciences, Beijing 100029

(Received 18 October 2011; revised 6 March 2012)

ABSTRACT

In this study, the relationship between the limit of predictability and initial error was investigated using two simple chaotic systems: the Lorenz model, which possesses a single characteristic time scale, and the coupled Lorenz model, which possesses two different characteristic time scales. The limit of predictability is defined here as the time at which the error reaches 95% of its saturation level; nonlinear behaviors of the error growth are therefore involved in the definition of the limit of predictability. Our results show that the logarithmic function performs well in describing the relationship between the limit of predictability and initial error in both models, although the coefficients in the logarithmic function were not constant across the examined range of initial errors.

Compared with the Lorenz model, in the coupled Lorenz model—in which the slow dynamics and the fast dynamics interact with each other—there is a more complex relationship between the limit of predictability and initial error. The limit of predictability of the Lorenz model is unbounded as the initial error becomes infinitesimally small; therefore, the limit of predictability of the Lorenz model may be extended by reducing the amplitude of the initial error. In contrast, if there exists a fixed initial error in the fast dynamics of the coupled Lorenz model, the slow dynamics has an intrinsic finite limit of predictability that cannot be extended by reducing the amplitude of the initial error in the slow dynamics, and vice versa. The findings reported here reveal the possible existence of an intrinsic finite limit of predictability in a coupled system that possesses many scales of time or motion.

Key words: limit of predictability, initial error, Lorenz model, coupled Lorenz model

Citation: Ding, R. Q., and J. P. Li, 2012: Relationships between the limit of predictability and initial error in the uncoupled and coupled Lorenz models. *Adv. Atmos. Sci.*, **29**(5), 1078–1088, doi: 10.1007/s00376-012-1207-8.

1. Introduction

Chaotic systems are characterized by a "sensitive dependence on initial conditions" (Eckmann and Ruelle, 1985), such that the predictability of future states is often severely limited by the chaotic dynamics of the system. In the pioneering work of Lorenz (1969a), geophysical systems are classified into three categories according to the general behavior of the limit of predictability. Systems in the first category have an infinite limit of predictability no matter how large the initial error. Systems in the second category have a finite limit, but this limit may be increased indefinitely by reducing the size of the initial error. Systems in the third category have an intrinsic finite limit of predictability that cannot be lengthened by reducing the amplitude of the initial error. By definition, chaotic systems fall into one of the latter two categories. It has long been assumed that deterministic fluid systems that possess many scales of motion, such as the atmosphere, have an intrinsic finite limit of predictability due to the cascade of prediction errors from small to large scales (Lorenz, 1969a; Leith, 1971; Leith and Kraichnan, 1972; Metais and Lesieur, 1986).

The sensitive dependence of chaotic systems on initial conditions indicates a close relationship between the limit of predictability and initial error. Lorenz (1969a) described the general behavior of the change

*Corresponding author: DING Ruiqiang, drq@mail.iap.ac.cn

in the limit of predictability as a function of initial error, but he did not provide a detailed analysis of the relationship between the limit of predictability and initial error.

In studies of nonlinear dynamical systems, Lyapunov exponents measure the average exponential rates of divergence or convergence of nearby orbits on a strange attractor and thus quantify the average predictability of a chaotic system (Oseledec, 1968). By definition, if the initial perturbation is of the size E_0 and the accepted error tolerance Δ remains small, then the maximal Lyapunov exponent λ_1 of a chaotic system determines a logarithmic relationship between the predictability time $T_{\rm P}$ and E_0 (Eckmann and Ruelle, 1985; Wolf et al., 1985; Lorenz, 1996):

$$T_{\rm p} \sim \frac{1}{\lambda_1} \ln \left(\frac{\Delta}{E_0} \right) , \qquad (1)$$

so that $T_{\rm P}$ decreases at a rate of $1/\lambda_1$ with increasing $\ln E_0$. However, for the predictability time Eq. (1) holds only for infinitesimal perturbations and in nonintermittent systems (Boffetta et al., 1998; Ding et al., 2006; Ding and Li, 2007; Li and Ding, 2011a). In addition, Boffetta et al. (1998) showed that the maximal Lyapunov exponent is not sufficient to estimate the predictability time for systems with different characteristic time scales. Consequently, Eq. (1) performs poorly in describing the relationship between the limit of predictability and initial error in the case of large initial errors or in systems with different characteristic time scales.

The potential existence of an inherent limit of atmospheric predictability has been a question of great concern in recent decades. The predictability of weather has long been recognized to be inherently limited because of the chaotic nature of the atmosphere (Lorenz, 1963, 1965; Chou, 1989; Simmons et al., 1995; Mu et al., 2002; Zhou, 2005; Palmer, 2006). Several studies have examined the relationship between the limit of predictability (the time taken for the initial error to reach the climate noise level) and initial error for the atmosphere. Chen (1989) and Toth (1991) assumed a linear relationship between the limit of predictability and initial error. They concluded from this linear relationship that the limit of predictability for an infinitesimal initial error in the observed atmosphere is ∼2 weeks. Nohara and Tanaka (2001) later showed that the relationship between the limit of predictability and initial error in a barotropic model of the atmosphere is logarithmic rather than linear, implying that the predictability for the model atmosphere is theoretically unbounded. Nohara and Tanaka (2001) then applied the logarithmic relationship from the barotropic model to the observed atmosphere. They concluded that the predictability of the barotropic component of the atmosphere could be extended by reducing the initial error in the vertical mean component of the atmosphere.

Observed atmospheric data contain almost all of the real information regarding the day-to-day movement and evolution of weather systems. It is appropriate to investigate the real atmospheric predictability based on observational data. Estimation of atmospheric predictability based on circulation analogues has been discussed in previous studies (Lorenz, 1969b; van den Dool, 1994). However, owing to the relatively short observational record of the atmosphere, it is difficult to find good analog pairs to investigate the error growth for a sufficiently small initial error (Lorenz, 1969b; van den Dool, 1994). According to van den Dool (1994), it would take a data library on the order of 10^{30} years to find good global analogues over a large region such as the Northern Hemisphere (where the number of spatial degrees of freedom is large). Obviously, it is impossible to find good global analogues with current libraries of historical atmospheric data that span 10 to 100 years. In addition, numerical models in use today provide imperfect simulations of the observed atmosphere, and model deficiencies strongly influence estimates of atmospheric predictability. Therefore, this study does not attempt to determine whether the relationship between the limit of predictability and initial error is linear or logarithmic for the observed atmosphere. Instead, we investigate the relationship between the limit of predictability and initial error in two simple chaotic systems: the Lorenz model that possesses a single characteristic time scale, and the coupled Lorenz model that possesses two different characteristic time scales. By comparing and contrasting how the limit of predictability varies as a function of initial errors in these two models, we tested whether a coupled model with different time scales have an intrinsic finite limit of predictability that does not depend on errors in the initial conditions. The results of this study revealed the influences of interactions among different time scales on the limit of predictability in a coupled model that possesses many scales of time or motion.

In the present study, the limit of predictability is defined as the time at which the error reaches 95% of its saturation level. Because error growth is nonlinear as the error reaches a large value and gradually approaches saturation, the nonlinear behaviors of the error growth are involved in the definition of the limit of predictability (Dalcher and Kalnay, 1987; Krishnamurthy, 1993; Li and Ding, 2011a). The limits of predictability for initial errors of various magnitudes (from small to large) can therefore be determined for

both the uncoupled and coupled Lorenz models. Equation (1) can be extended to account for large initial errors and coupled systems with different characteristic time scales.

Notably, the present study is an extension of our previous research (Li and Ding, 2011b) in which we presented a linear relationship between the limit of predictability and the logarithm of sufficiently small initial errors for the Lorenz model. The behaviors of the limit of predictability for larger initial errors and for the coupled model were not addressed in Li and Ding (2011b). The remainder of this paper is arranged as follows. In section 2, the limit of predictability for the Lorenz model is presented as a function of the initial error. In section 3, the limits of predictability for the slow dynamics and fast dynamics in the coupled Lorenz model are presented as functions of the initial errors. Concluding remarks are given in section 4.

2. The Lorenz model with a single time scale

The first example is given by the Lorenz model (Lorenz, 1963):

$$\begin{cases} \dfrac{dX_1}{dt} = -\sigma X_1 + \sigma X_2 \,, \\ \dfrac{dX_2}{dt} = rX_1 - X_2 - X_1X_3 \,, \\ \dfrac{dX_3}{dt} = X_1X_2 - bX_3 \,, \end{cases} \tag{2}$$

where σ, r, and b are parameters that represent the Prandtl number, the Rayleigh number, and a geometric factor, respectively. The state variables, X_1, X_2, and X_3 represent measures of fluid velocity and the spatial temperature distribution in the fluid layer under gravity. The parameters have the values σ=10, r=28, and b=8/3, for which the well-known "butterfly" attractor exists. The maximal Lyapunov exponent of the Lorenz model with these parameters is λ_1=0.905 (Shimada and Nagashima, 1979; Benettin et al., 1980). A long integration using the fourth-order Runge–Kutta method with a time stepsize h=0.01 was performed to obtain 8×10^4 points within the attractor, which represent an ensemble of initial unperturbed states. A set of random errors, which have a Gaussian distribution with zero mean and magnitude E_0, were superimposed on the unperturbed states to form an ensemble of perturbed states. The magnitude E_0 of the individual error is simply the root-mean-square distance (RMSD) between the perturbed and the unperturbed states in the three-dimensional phase space. An ensemble of 8×10^4 errors at each time step was obtained by integrating solutions of the Lorenz model that originated from the unperturbed and perturbed initial states. The ensemble average of the magnitude of the errors was defined as the average error E. The ensemble average was taken as the geometric mean.

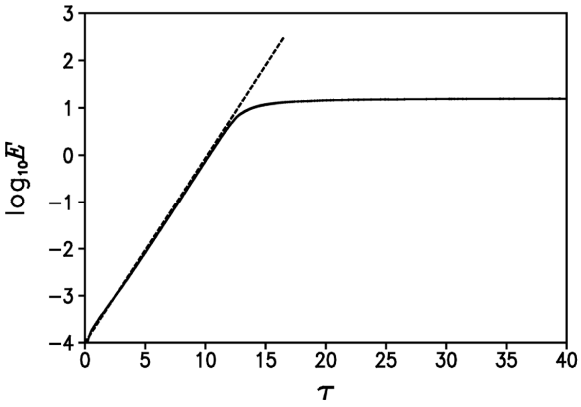

Fig. 1. Average growth of errors with initial magnitude $E_0 = 10^{-4}$ in the Lorenz model. The dashed lines indicate the exponential growth of errors with the growth rate λ_1=0.905. λ_1 is the maximal Lyapunov exponent of the Lorenz model.

Figure 1 presents the ensemble average growth of errors with initial magnitude $E_0 = 10^{-4}$. At the early stage, the error growth was exponential, with a growth rate consistent with the maximal Lyapunov exponent λ_1, indicating that linear error dynamics are applicable during this phase. When the magnitude of the error was nearly $10^{0.2}$, the error growth started to deviate from the exponential growth. The error growth then entered a nonlinear phase with a steadily decreasing growth rate, finally reaching a saturation value. For large initial errors, such as $E_0 = 10$, the exponential growth phase was absent, and the error growth entered directly into the nonlinear phase, with a growth rate less than λ_1 (not shown). Once the error growth reached the saturation level, almost all information on initial states was lost, and prediction became meaningless. The limit of predictability $T_{\rm p}$ is defined as the time at which the error reaches 95% of its saturation level. We found that $T_{\rm p}$=23.04 for the Lorenz model with $E_0 = 10^{-4}$.

Figure 2 shows the limits of predictability $T_{\rm p}$ as a function of $\lg E_0$. $T_{\rm p}$ decreased approximately linearly with increasing $\lg E_0$ for $E_0<10^{0.2}$; however, $T_{\rm p}$ decreased more quickly than linearly with increasing $\lg E_0$ for $E_0 \geqslant 10^{0.2}$. As discussed previously regarding Fig. 1, the tangent linear approximation of error growth was no longer valid, and the error growth entered a nonlinear phase when the error growth reached nearly $10^{0.2}$. Therefore, we conclude that the relationship between the limit of predictability and initial error for small E_0 ($< 10^{0.2}$) may be different from that for large E_0 ($\geqslant 10^{0.2}$).

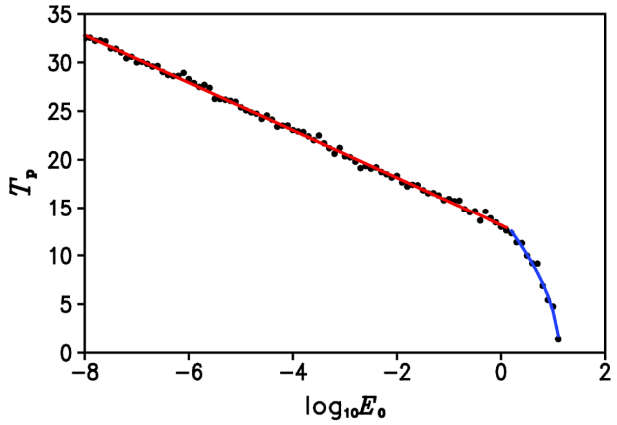

Fig. 2. Scatter diagram of the limit of predictability $T_{\rm P}$ versus $\lg E_0$ in the Lorenz model. The red line is the curve fit by regression of the data shown by the solid circles using Eq. (7) for $E_0<10^{0.2}$. The blue line is the curve fit by regression of the data shown by the solid circles using Eq. (7) for $E_0 \geqslant 10^{0.2}$.

Lorenz (1982) introduced a crude formula to describe the average growth of error E in chaotic systems:

$$\frac{dE}{dt} = \alpha E - \frac{\alpha}{E_\infty} E^2 \,, \tag{3}$$

where E_∞ denotes the saturation value for E and α is an exponential growth rate for small error. This error equation considers both an exponential growth of small errors (with a growth rate of α) and the saturation effect of large errors at sufficiently long times. If E_0 is the initial error at time t_0, then the error E at a later time t is given by Store and Royer (1993):

$$E = \frac{E_\infty}{1 + \left(\dfrac{E_\infty}{E_0} - 1\right) e^{-\alpha t}} \,. \tag{4}$$

If the limit of predictability $T_{\rm P}$ is defined as the time taken for E to reach a critical value $E_{\rm l}$ below E_∞ (for example, 95% E_∞ as taken in this study), then $T_{\rm P}$ may be written using E_0:

$$T_{\rm P} = -\frac{1}{\alpha}\left\{\ln\left[\frac{E_0}{E_\infty - E_0}\right] + \ln\left[\frac{E_\infty - E_{\rm l}}{E_{\rm l}}\right]\right\}. \tag{5}$$

Then Eq. (5) may be changed to the following form:

$$T_{\rm P} = -\frac{c}{\alpha}\left\{\lg\left[\frac{E_0}{E_\infty - E_0}\right] + \lg\left[\frac{E_\infty - E_{\rm l}}{E_{\rm l}}\right]\right\} \,, \tag{6}$$

where c is a constant equal to 2.303. According to Eq. (6), the relationship between $T_{\rm P}$ and $\lg E_0$ is linear when E_0 is sufficiently small, and $T_{\rm P}$ decreases more and more quickly as E_0 gradually approaches E_∞.

For various E_0, we computed the limit of predictability $T_{\rm P}$ according to Eq. (6) with $\alpha = \lambda_1$ and

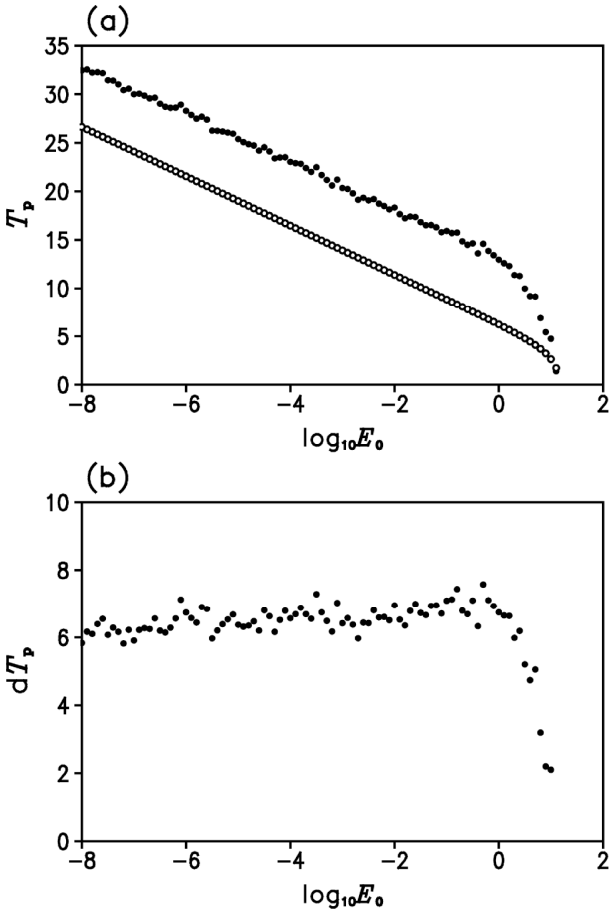

Fig. 3. (a) Scatter diagram of the limit of predictability shown in Fig. 2 (denoted $T_{\rm P0}$; closed circles) and the limit of predictability obtained using the empirical formula given by Eq. (6) with α=0.905 and E_l=95%E_∞ (denoted $T_{\rm P1}$; open circles) versus $\lg E_0$ in the Lorenz model. (b) Scatter diagram of the difference between $T_{\rm P0}$ and $T_{\rm P1}$ versus $\lg E_0$.

$E_{\rm l}$=95% E_∞. The limits of predictability $T_{\rm P}$ according to Eq. (6) (denoted $T_{\rm P1}$) and as shown in Fig. 2 (denoted $T_{\rm P0}$), are presented in Fig. 3a. For $E_0<10^{0.2}$, $T_{\rm P1}$ decreased approximately linearly with increasing $\lg E_0$, at a rate similar to that of $T_{\rm P0}$; however, there was a significant difference between $T_{\rm P0}$ and $T_{\rm P1}$ that remained almost constant (Fig. 3b). The reason for this constant difference between $T_{\rm P0}$ and $T_{\rm P1}$ is that although the empirical error E according to Eq. (4) describes the exponential growth phase quite well, it fails to describe the nonlinear phase of the error growth. The empirical error saturated more quickly than the actual error (Fig. 4), thereby resulting in a smaller limit of predictability. The difference between the empirical and actual limits of predictability was roughly constant for small initial errors. Accordingly, the empirical formula given by Eq. (6) seems a good approximation for the limit of predictability for small initial

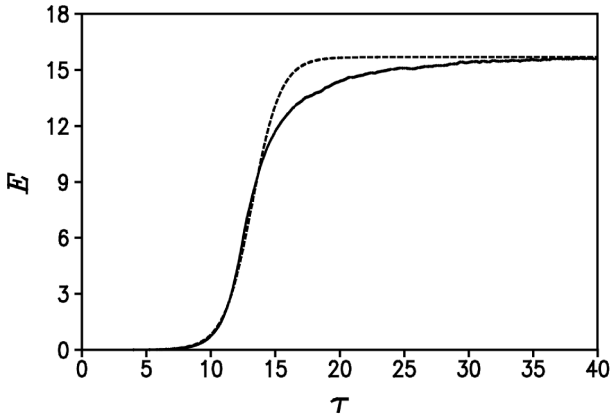

Fig. 4. The dashed curve shows the error growth according to the empirical formula given by Eq. (4) with α=0.905 and $E_0 = 10^{-4}$. The solid curve shows the average error growth with $E_0 = 10^{-4}$ as shown in Fig. 1. To highlight the difference between the two curves, the error E is used instead of $\lg E$ as the y coordinate.

errors, provided that a constant is added to the right side of the equation.

For $E_0 \geqslant 10^{0.2}$, the decreasing rate of T_{P1} with $\lg E_0$ was less than that of T_{P0}, so that the difference between T_{P0} and T_{P1} gradually decreased with increasing $\lg E_0$ (Fig. 3b). In fact, a better fit to the curve of T_{P0} for $E_0 \geqslant 10^{0.2}$ was obtained with Eq. (6) by choosing α=0.33 rather than $\alpha = \lambda_1$ [see Eq. (7)]. As shown in Eq. (7), the exponential growth rate of small E_0 ($< 10^{0.2}$) was close to the maximal Lyapunov exponent λ_1= 0.905, while that of large E_0 ($\geqslant 10^{0.2}$) was significantly less than λ_1. Similar results were found by Krishnamurthy (1993), who pointed out that the growth rate of large initial errors cannot be interpreted in terms of the Lyapunov exponents in the Lorenz's 28-variable model.

Based on our results, the relationship between the limit of predictability and initial error in the Lorenz model can result from the logarithmic regression using Eq. (6) for small E_0 ($< 10^{0.2}$) and large E_0 ($\geqslant 10^{0.2}$), respectively,

$$\begin{cases} T_{\mathrm{P}} = -\dfrac{c}{0.94} \lg \dfrac{E_0}{E_\infty - E_0} + 10.29 \,, \\ \qquad \text{if } E_0 < 10^{0.2} \\ T_{\mathrm{P}} = -\dfrac{c}{0.33} \lg \dfrac{E_0}{E_\infty - E_0} + 5.93 \,, \\ \qquad \text{if } 10^{0.2} \leqslant E_0 < E_\infty \end{cases} \tag{7}$$

where c=2.303 and E_∞=15.69. The fitting curve using Eq. (7) is shown in Fig. 2. According to Eq. (7), T_{P} can be extended by ~2.45 when E_0 decreases to $E_0/10$ for sufficiently small E_0. The logarithmic relationship implies that T_{P} is unbounded as E_0 approaches 0. We can extend the limit of predictability as long as we can reduce the initial error.

3. The coupled Lorenz model with two different time scales

The example presented in section 2 is the Lorenz model with a single characteristic time scale. Next, we discuss the relationship between the limit of predictability and initial error in the coupled Lorenz model with different characteristic time scales. The coupled Lorenz model was obtained by coupling two Lorenz models, with the first representing the slow dynamics and the second the fast dynamics (Boffetta et al., 1998):

$$\begin{cases} \dfrac{dX_1^{(\mathrm{s})}}{dt} = \sigma(X_2^{(\mathrm{s})} - X_1^{(\mathrm{s})}) \,, \\ \dfrac{dX_2^{(\mathrm{s})}}{dt} = \left(-X_1^{(\mathrm{s})} X_3^{(\mathrm{s})} + r_s X_1^{(\mathrm{s})} - X_2^{(\mathrm{s})}\right) - \\ \qquad \varepsilon_s X_1^{(\mathrm{f})} X_2^{(\mathrm{f})} \,, \\ \dfrac{dX_3^{(\mathrm{s})}}{dt} = X_1^{(\mathrm{s})} X_2^{(\mathrm{s})} - b X_3^{(\mathrm{s})} \,, \\ \dfrac{dX_1^{(\mathrm{f})}}{dt} = c\sigma(X_2^{(\mathrm{f})} - X_1^{(\mathrm{f})}) \,, \\ \dfrac{dX_2^{(\mathrm{f})}}{dt} = c(-X_1^{(\mathrm{f})} X_3^{(\mathrm{f})} + r_f X_1^{(\mathrm{f})} - X_2^{(\mathrm{f})}) + \\ \qquad \varepsilon_f X_1^{(\mathrm{f})} X_2^{(\mathrm{s})} \,, \\ \dfrac{dX_3^{(\mathrm{f})}}{dt} = c(X_1^{(\mathrm{f})} X_2^{(\mathrm{f})} - b X_3^{(\mathrm{f})}) \,, \end{cases} \tag{8}$$

where the superscripts (s) and (f) denote the slow dynamics and the fast dynamics, respectively. In the coupled Lorenz model, the parameters have the values σ=10, b=8/3, and c=10, the last implying that the fast dynamics tends to fluctuate 10 times as quickly as the slow dynamics. The Rayleigh numbers of the slow dynamics and the fast dynamics were taken differently, r_{s}=28 and r_{f}=45 for generality. When the coupling coefficients ε_{s} and ε_{f} equal 0, the uncoupled fast and slow Lorenz models display chaotic behavior with the maximal Lyapunov exponents $\lambda_1^{(\mathrm{f})}$=12.17 and $\lambda_1^{(\mathrm{s})}$=0.905, respectively. For $\varepsilon_{\mathrm{s}} = 10^{-2}$ and ε_{f}=10, Boffetta et al. (1998) showed that the coupled Lorenz model has the maximal Lyapunov exponent λ_1=11.5, which is close to $\lambda_1^{(\mathrm{f})}$ in the uncoupled case. This result indicates that the maximal Lyapunov exponent in a multi-scale system is mainly determined by the error growth of the fast dynamics.

In this study, we computed the error growth for the

coupled Lorenz model with the coupling coefficients as prescribed in Boffetta et al. (1998): $\varepsilon_{\rm s} = 10^{-2}$ and $\varepsilon_{\rm f}$=10. We obtained the solutions originating from the unperturbed and perturbed initial states by integrating the coupled Lorenz model using a time-step size of h=0.005. The perturbed initial states were subjected to random errors with magnitudes $E_0^{\rm (s)}$ and $E_0^{\rm (f)}$ on the unperturbed initial states of the slow dynamics and the fast dynamics, respectively. The errors of the slow dynamics and the fast dynamics (denoted as $E^{\rm (s)}$ and $E^{\rm (f)}$, respectively) were computed using the root-mean-square error (RMSE) between the unperturbed and perturbed initial states.

According to Boffetta et al. (1998, see their Fig. 2), when $E_0^{\rm (s)}$ and $E_0^{\rm (f)}$ is infinitesimally small, the fast dynamics in the coupled Lorenz model plays a dominant role in the rapid growth of $E^{\rm (s)}$; both $E^{\rm (f)}$ and $E^{\rm (s)}$ begin to grow at an exponential rate close to the maximal Lyapunov exponent $\lambda_1^{\rm (f)}$ of the fast dynamics. $E^{\rm (f)}$ quickly reaches saturation, but $E^{\rm (s)}$ continues to grow at a slower quasi-exponential rate comparable to its maximal Lyapunov exponent $\lambda_1^{\rm (s)}$. In this latter case, the slow dynamics in the coupled Lorenz model plays a dominant role in the growth of $E^{\rm (s)}$, while the fast dynamics is less relevant. The transition from fast growth to slow growth of $E^{\rm (s)}$ occurs when $E^{\rm (s)}$ grows more than 10^{-2}, which roughly corresponds to the magnitude of the coupling $\varepsilon_{\rm s}$. When the magnitude of $E^{\rm (s)}$ is nearly $10^{0.2}$, the growth of $E^{\rm (s)}$ enters a nonlinear phase with a steadily decreasing growth rate. Finally $E^{\rm (s)}$ approaches its own saturation level, which is slightly lower than that of $E^{\rm (f)}$. Therefore, 10^{-2} and $10^{0.2}$ are critical values of $E^{\rm (s)}$ that separate different phases of the error growth of the slow dynamics.

3.1 *Predictability limit of the slow dynamics*

We first investigated the influences of the coupling on the relationship between the predictability limit of the slow dynamics and its initial error $E_0^{\rm (s)}$. Here we studied two different cases. In the first case, no initial error existed in the fast dynamics (i.e., $E_0^{\rm (f)}$=0). In the second case, a fixed initial error with magnitude $E_0^{\rm (f)}$=10^{-8} existed in the fast dynamics. In both cases, $E_0^{\rm (s)}$ varied from 10^{-8} to $10^{1.1}$ (slightly below the saturation value of $E^{\rm (s)}$).

For the first case ($E_0^{\rm (f)}$=0), Fig. 5 shows the error growth of the slow dynamics for $E_0^{\rm (s)}$ of various magnitudes, averaged over 5×10^4 initial states. For small $E_0^{\rm (s)}$ ($< 10^{-2}$), the growth of $E^{\rm (s)}$ displayed two distinctly different phases: the first phase characterized the fast growth, while the latter phase characterized the slow growth, consistent with Boffetta et al. (1998).

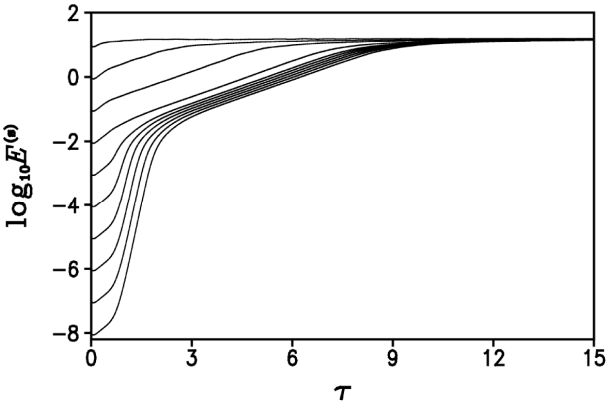

Fig. 5. Average error growth of the slow dynamics as a function of time τ and $E_0^{\rm (s)}$ in the coupled Lorenz model with $E_0^{\rm (f)}$=0. From below to above, the curves correspond to $E_0^{\rm (s)} = 10^{-8}$, 10^{-7}, 10^{-6}, 10^{-5}, 10^{-4}, 10^{-3}, 10^{-2}, 10^{-1}, 10^{0}, and 10, respectively.

For large $E_0^{\rm (s)}$ ($\geqslant 10^{-2}$), the fast-growth phase was absent and only the slow-growth phase was evident. The predictability limit of the slow dynamics (denoted as $T_{\rm P}^{\rm (s)}$) was defined as the time at which $E^{\rm (s)}$ reached 95% of its saturation level.

Figure 6a shows the dependence of $T_{\rm P}^{\rm (s)}$ on $\lg E_0^{\rm (s)}$. It is obvious that the decreasing rates of $T_{\rm P}^{\rm (s)}$ with increasing $\lg E_0^{\rm (s)}$ are different for different intervals of $E_0^{\rm (s)}$. For $E_0^{\rm (s)}$<10^{-2}, $T_{\rm P}^{\rm (s)}$ showed a slow, almost linear decrease with increasing $\lg E_0^{\rm (s)}$; for $10^{-2}\leqslant E_0^{\rm (s)}<10^{0.2}$, $T_{\rm P}^{\rm (s)}$ showed a quick, almost linear decrease with increasing $\lg E_0^{\rm (s)}$; for $10^{0.2}<E_0^{\rm (s)}<E_\infty^{\rm (s)}$ (where $E_\infty^{\rm (s)}$ is the saturation value of $E^{\rm (s)}$), $T_{\rm P}^{\rm (s)}$ decreased more and more quickly with increasing $\lg E_0^{\rm (s)}$. The regression between $T_{\rm P}^{\rm (s)}$ and $E_0^{\rm (s)}$ using Eq. (6) yielded a piecewise function for different intervals of $E_0^{\rm (s)}$:

$$\begin{cases} T_{\rm P}^{\rm (s)} = -\dfrac{c}{11.92}\lg\dfrac{E_0^{\rm (s)}}{E_\infty^{\rm (s)}-E_0^{\rm (s)}} + 16.61\,, \\ \qquad \text{if } E_0^{\rm (s)} < 10^{-2} \\ T_{\rm P}^{\rm (s)} = -\dfrac{c}{1.07}\lg\dfrac{E_0^{\rm (s)}}{E_\infty^{\rm (s)}-E_0^{\rm (s)}} + 10.42\,, \\ \qquad \text{if } 10^{-2} \leqslant E_0^{\rm (s)} < 10^{0.2} \\ T_{\rm P}^{\rm (s)} = -\dfrac{c}{0.31}\lg\dfrac{E_0^{\rm (s)}}{E_\infty^{\rm (s)}-E_0^{\rm (s)}} + 5.76\,, \\ \qquad \text{if } 10^{0.2} \leqslant E_0^{\rm (s)} < E_\infty^{\rm (s)} \end{cases} \tag{9}$$

where c=2.303 and $E_\infty^{\rm (s)}$=15.46. The fitting curve using Eq. (9) is shown in Fig. 6a. Using Eq. (9), the value

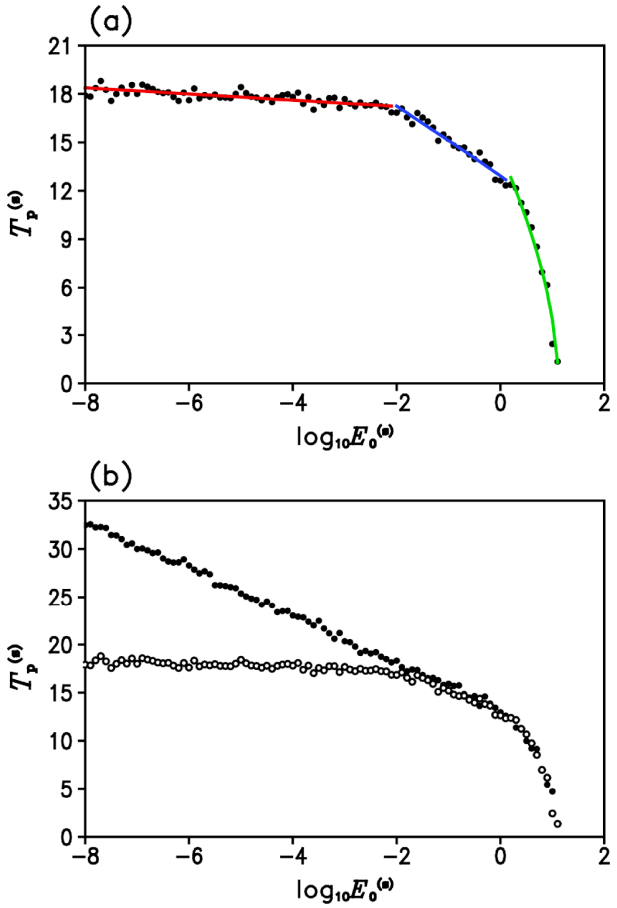

Fig. 6. (a) Scatter diagram of the limit of predictability of the slow dynamics $T_{\mathrm{P}}^{(\mathrm{s})}$ versus $\lg E_0^{(\mathrm{s})}$ in the coupled Lorenz model with $E_0^{(\mathrm{f})}$=0. The red, blue, and green lines are the curves fitted by the regression of the data shown by the solid circles using Eq. (9) for $E_0^{(\mathrm{s})} < 10^{-2}$, $10^{-2} \leqslant E_0^{(\mathrm{s})} < 10^{0.2}$, and $10^{0.2} \leqslant E_0^{(\mathrm{s})} < E_\infty^{(\mathrm{s})}$, respectively. (b) Open circles correspond to the limits of predictability of the coupled slow dynamics as a function of $\lg E_0^{(\mathrm{s})}$, while closed circles correspond to those of the uncoupled slow dynamics.

of α [which corresponded to the exponential growth rate of error in Eq. (6)] was close to $\lambda_1^{(\mathrm{f})}$ for $E_0^{(\mathrm{s})} < 10^{-2}$, while it was close to $\lambda_1^{(\mathrm{s})}$ for $10^{-2} \leqslant E_0^{(\mathrm{s})} < 10^{0.2}$.

A comparison of Eq. (7) and Eq. (9) showed that the changes of $T_{\mathrm{P}}^{(\mathrm{s})}$ with $E_0^{(\mathrm{s})}$ in the coupled Lorenz model are similar to those in the uncoupled Lorenz model for $E_0^{(\mathrm{s})} \geqslant 10^{-2}$ (Fig. 6b). However, for $E_0^{(\mathrm{s})} < 10^{-2}$, the changes of $T_{\mathrm{P}}^{(\mathrm{s})}$ with $E_0^{(\mathrm{s})}$ were dominated by the fast dynamics, leading to a slower increase of $T_{\mathrm{P}}^{(\mathrm{s})}$ with decreasing $\lg E_0^{(\mathrm{s})}$. As $E_0^{(\mathrm{s})}$ became infinitesimally small, the reduction in the predictability of the slow dynamics due to the coupling with the fast dynamics became more pronounced. According to Eq. (9), $T_{\mathrm{P}}^{(\mathrm{s})}$ was unbounded as $E_0^{(\mathrm{s})}$ approaches 0; however, $T_{\mathrm{P}}^{(\mathrm{s})}$ is only extended by ∼0.19 when $E_0^{(\mathrm{s})}$ decreased to $E_0^{(\mathrm{s})}/10$ for sufficiently small $E_0^{(\mathrm{s})}$. This result indicates that it is difficult to extend the predictability limit of the slow dynamics in the coupled Lorenz model by reducing the initial error $E_0^{(\mathrm{s})}$.

For the second case ($E_0^{(\mathrm{f})}$=10^{-5}), the average error-growth curves of the slow dynamics as a function of time τ and $E_0^{(\mathrm{s})}$ are shown in Fig. 7. A comparison of Fig. 5 and Fig. 7 shows that the error growth curves in the second case mainly differed from those in the first case for $E_0^{(\mathrm{s})} \leqslant 10^{-5}$. With $E_0^{(\mathrm{f})}$=10^{-5}, the curves of $E^{(\mathrm{s})}$ with $E_0^{(\mathrm{s})} \leqslant 10^{-5}$ tended to overlay each other as τ increases. The curves began to separate as $E_0^{(\mathrm{s})}$ exceeded 10^{-5}, and the time that $E^{(\mathrm{s})}$ reached saturation shortens as $E_0^{(\mathrm{s})}$ increases. Consistent with these error growth of the slow dynamics, $T_{\mathrm{P}}^{(\mathrm{s})}$ remained almost constant with increasing $\lg E_0^{(\mathrm{s})}$ for $E_0^{(\mathrm{s})} \leqslant 10^{-5}$ (Fig. 8). For $E_0^{(\mathrm{s})} > 10^{-5}$, $T_{\mathrm{P}}^{(\mathrm{s})}$ gradually decreased with increasing $\lg E_0^{(\mathrm{s})}$, although the rate of decrease differed for different intervals of $E_0^{(\mathrm{s})}$. The regression between $T_{\mathrm{P}}^{(\mathrm{s})}$ and $E_0^{(\mathrm{s})}$ using Eq. (6) yields

$$\begin{cases} T_{\mathrm{P}}^{(\mathrm{s})} = 17.69, \text{ if } E_0^{(\mathrm{s})} \leqslant 10^{-5}\,, \\ T_{\mathrm{P}}^{(\mathrm{s})} = -\dfrac{c}{11.92} \lg \dfrac{E_0^{(\mathrm{s})}}{E_\infty^{(\mathrm{s})} - E_0^{(\mathrm{s})}} + 16.62\,, \\ \qquad \text{if } 10^{-5} < E_0^{(\mathrm{s})} < 10^{-2} \\ T_{\mathrm{P}}^{(\mathrm{s})} = -\dfrac{c}{1.11} \lg \dfrac{E_0^{(\mathrm{s})}}{E_\infty^{(\mathrm{s})} - E_0^{(\mathrm{s})}} + 10.54\,, \\ \qquad \text{if } 10^{-2} \leqslant E_0^{(\mathrm{s})} < 10^{0.2} \\ T_{\mathrm{P}}^{(\mathrm{s})} = -\dfrac{c}{0.33} \lg \dfrac{E_0^{(\mathrm{s})}}{E_\infty^{(\mathrm{s})} - E_0^{(\mathrm{s})}} + 5.62\,, \\ \qquad \text{if } 10^{0.2} \leqslant E_0^{(\mathrm{s})} < E_\infty^{(\mathrm{s})} \end{cases} \tag{10}$$

where c=2.303 and $E_\infty^{(\mathrm{s})}$=15.46. The fitting curve using Eq. (10) is shown in Fig. 8. According to Eq. (10), if the fast dynamics has a small initial error with magnitude equal to 10^{-5}, the predictability of the slow dynamics is limited to ∼17.69. In this case, the slow dynamics has an intrinsic finite limit of predictability, which could not be extended by reducing the amplitude of initial errors of the slow dynamics. When $E_0^{(\mathrm{s})} > 10^{-5}$, the changes of the exponential growth rate α with $E_0^{(\mathrm{s})}$ using Eq. (10) were similar to those using Eq. (9), with the value close to $\lambda_1^{(\mathrm{f})}$ for $10^{-5} < E_0^{(\mathrm{s})} < 10^{-2}$ and close to $\lambda_1^{(\mathrm{s})}$ for $10^{-2} \leqslant E_0^{(\mathrm{s})} \leqslant 10^{0.2}$.

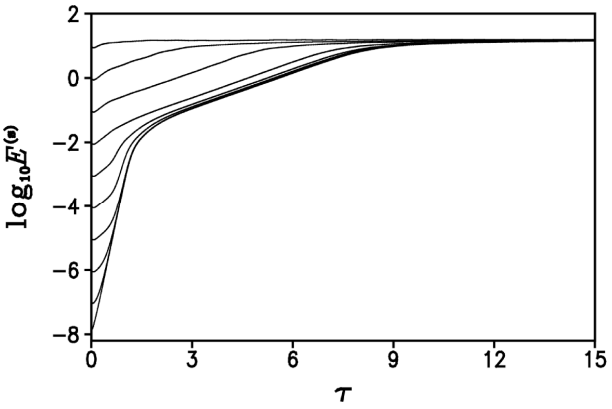

Fig. 7. Same as Fig. 5, but with $E_0^{(\mathrm{f})} = 10^{-5}$ in the coupled Lorenz model.

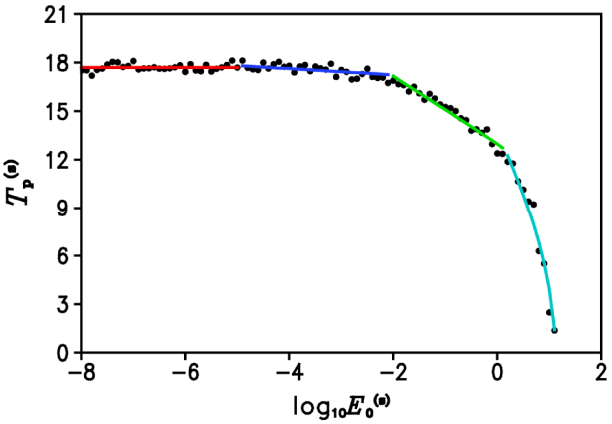

Fig. 8. Scatter diagram of the predictability limit of the slow dynamics $T_{\mathrm{P}}^{(\mathrm{s})}$ versus $\lg E_0^{(\mathrm{s})}$ in the coupled Lorenz model with $E_0^{(\mathrm{f})} = 10^{-5}$. The red, dark blue, green, and light blue lines are the curves fitted by the regression of the data shown by the solid circles using Eq. (10) for $E_0^{(\mathrm{s})} \leqslant 10^{-5}$, $10^{-5} < E_0^{(\mathrm{s})} < 10^{-2}$, $10^{-2} \leqslant E_0^{(\mathrm{s})} < 10^{0.2}$, and $10^{0.2} \leqslant E_0^{(\mathrm{s})} < E_\infty^{(\mathrm{s})}$, respectively.

The relationship between $T_{\mathrm{P}}^{(\mathrm{s})}$ and $E_0^{(\mathrm{s})}$ described by Eq. (10) holds for any given $E_0^{(\mathrm{f})}$ with a value $< 10^{-2}$, but with a different upper bound of the predictability limit. For $E_0^{(\mathrm{f})} > 10^{-2}$, however, the maximal Lyapunov exponent $\lambda_1^{(\mathrm{f})}$ of the fast dynamics is no longer relevant to the relationship between $T_{\mathrm{P}}^{(\mathrm{s})}$ and $E_0^{(\mathrm{s})}$. In this case, the phase during which $T_{\mathrm{P}}^{(\mathrm{s})}$ decreased with increasing $\lg E_0^{(\mathrm{s})}$ at a rate close to $c/\lambda_1^{(\mathrm{f})}$ was absent (not shown).

3.2 *Predictability limit of the fast dynamics*

We next focused on the relationship between the predictability limit of the coupled fast dynamics and its initial error $E_0^{(\mathrm{f})}$. Similar to the slow dynamics, we considered two cases with different magnitudes for $E_0^{(\mathrm{s})}$. In these two cases, the initial errors of the slow dynamics were fixed at $E_0^{(\mathrm{s})}=0$ and $E_0^{(\mathrm{s})} = 10^{-5}$, respectively, and we investigated the dependence of the error growth and predictability of the fast dynamics on $E_0^{(\mathrm{f})}$. We varied $E_0^{(\mathrm{f})}$ between 10^{-8} and $10^{1.3}$ (slightly below the saturation value of $E^{(\mathrm{f})}$).

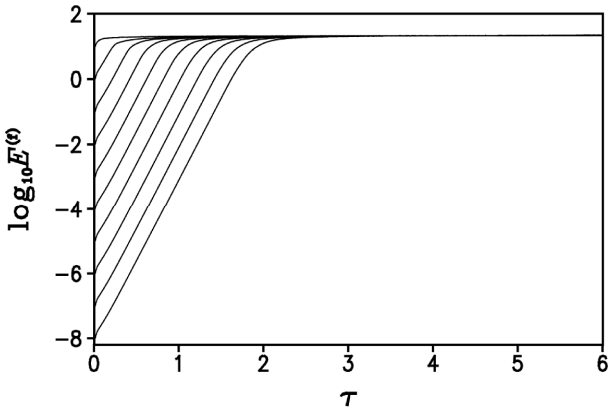

Fig. 9. Average error growth of the fast dynamics as a function of time τ and $E_0^{(\mathrm{f})}$ in the coupled Lorenz model with $E_0^{(\mathrm{s})}=0$. From below to above, the curves correspond to $E_0^{(\mathrm{f})}=10^{-8}$, 10^{-7}, 10^{-6}, 10^{-5}, 10^{-4}, 10^{-3}, 10^{-2}, 10^{-1}, 10^{0}, and 10, respectively.

For the first case ($E_0^{(\mathrm{s})}=0$), the average error growth of the fast dynamics is shown for $E_0^{(\mathrm{f})}$ of various magnitudes in Fig. 9. For small $E_0^{(\mathrm{f})}$, $E^{(\mathrm{f})}$ showed a quick increase in the early phase, after which it showed a slow increase until saturation. This result indicates that the fast dynamics play an important role in determining the initial error growth of $E^{(\mathrm{f})}$, while the error growth is more strongly influenced by the slow dynamics as $E^{(\mathrm{f})}$ increases. Compared with the error growth of the uncoupled fast dynamics (not shown), the coupling with the slow dynamics led to an extension of the time before $E^{(\mathrm{f})}$ reached saturation. As a result, the predictability limit $T_{\mathrm{P}}^{(\mathrm{f})}$ of the coupled fast dynamics was significantly greater than that of the uncoupled fast dynamics for all investigated magnitudes of $E_0^{(\mathrm{f})}$ (Fig. 10b). The predictability limit of the uncoupled fast dynamics showed an almost linear decrease with increasing $\lg E_0^{(\mathrm{f})}$ for $E_0^{(\mathrm{f})} < 10^{0.5}$ and a quicker than linear decrease with increasing $\lg E_0^{(\mathrm{f})}$ for $10^{0.5} \leqslant E_0^{(\mathrm{f})} < E_\infty^{(\mathrm{f})}$. By contrast, the predictability limit of the coupled fast dynamics showed an almost linear decrease with increasing $\lg E_0^{(\mathrm{f})}$ for $E_0^{(\mathrm{f})} < E_\infty^{(\mathrm{f})}$. When $E_0^{(\mathrm{f})}$ was close to its saturation level $E_\infty^{(\mathrm{f})}$, the predictability limit of the uncoupled fast dynamics approached 0; however, the predictability limit of the

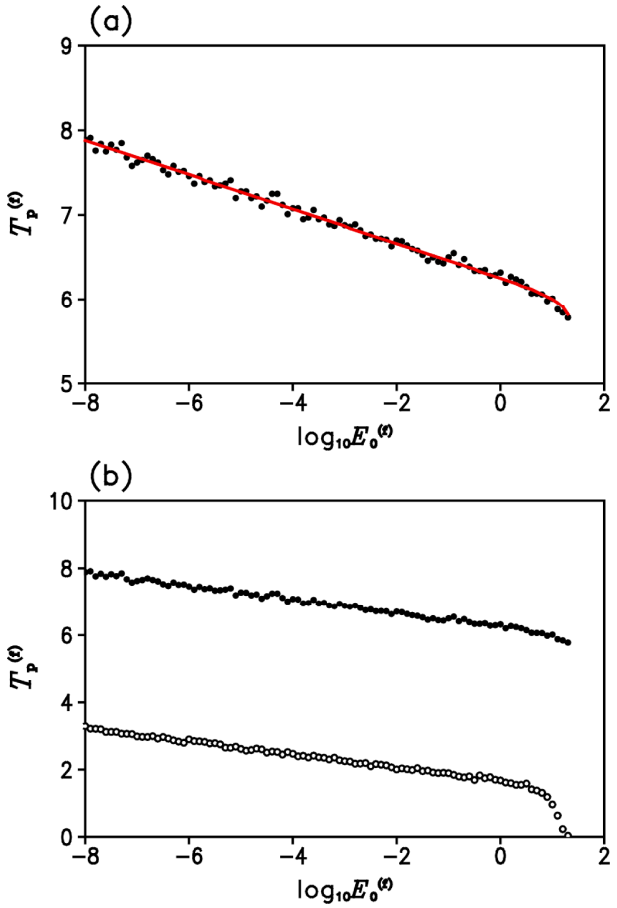

Fig. 10. (a) Scatter diagram of the limit of predictability of the fast dynamics $T_{\rm P}^{(\rm f)}$ versus $\lg E_0^{(\rm f)}$ in the coupled Lorenz model with $E_0^{(\rm s)}$=0. The red line is the curve fitted by the regression of the data shown by the solid circles using Eq. (11) for $E_0^{(\rm f)}<E_\infty^{(\rm f)}$. (b) Open circles correspond to the predictability limits of the uncoupled fast dynamics as a function of $\lg E_0^{(\rm f)}$, while closed circles correspond to those of the coupled fast dynamics.

coupled fast dynamics was ∼5.77. The regression between the predictability limit $T_{\rm P}^{(\rm f)}$ of the coupled fast dynamics and $E_0^{(\rm f)}$ using Eq. (6) yields

$$T_{\rm P}^{(\rm f)} = -\frac{c}{11.3}\lg\frac{E_0^{(\rm f)}}{E_\infty^{(\rm f)}-E_0^{(\rm f)}} + 5.98\,,$$
$$\text{if } E_0^{(\rm f)} < E_\infty^{(\rm f)}\,, \qquad (11)$$

where c=2.303 and $E_\infty^{(\rm f)}$=23.53. The fitting curve using Eq. (11) is shown in Fig. 11. According to Eq. (11), $T_{\rm P}^{(\rm f)}$ decreased with increasing $\lg E_0^{(\rm f)}$ at a rate close to $c/\lambda_1^{(\rm f)}$ and was unbounded as $E_0^{(\rm f)}$ approached 0.

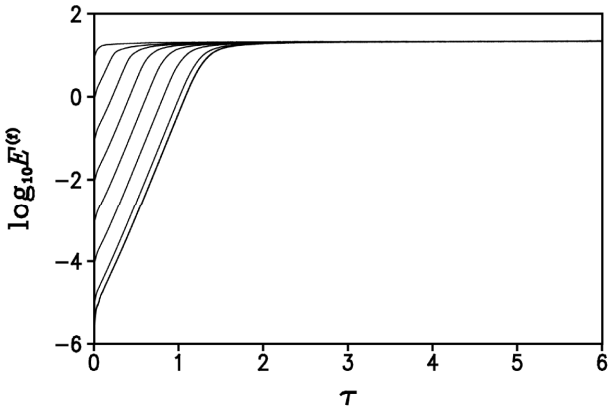

Fig. 11. Same as Fig. 9, but with $E_0^{(\rm s)} = 10^{-5}$ in the coupled Lorenz model.

For the second case ($E_0^{(\rm s)} = 10^{-5}$), the average error growth of the fast dynamics is shown in Fig. 11 for $E_0^{(\rm f)}$ of various magnitudes. For $E_0^{(\rm f)}\leqslant 10^{-6}$, the curves of $E^{(\rm f)}$ overlapped each other and could not be distinguished. When $E_0^{(\rm f)}$ increased to 10^{-5}, the curve of $E^{(\rm f)}$ slightly departed from the curves for $E_0^{(\rm f)}\leqslant 10^{-6}$. When $E_0^{(\rm f)}$ exceeded 10^{-5}, the curves of $E^{(\rm f)}$ showed significant separation, and the time before $E^{(\rm f)}$ reached saturation shortened as $E_0^{(\rm f)}$ increased. As $E_0^{(\rm f)}$ approached the saturation value $E_\infty^{(\rm f)}$, $E^{(\rm f)}$ did not increase initially but decayed temporarily for a short time interval, and then increased slowly to reach saturation (not shown). Therefore, a predictability limit >0 remained for large $E_0^{(\rm f)}$, which resulted mainly from the coupling with the slow dynamics. Figure 12 shows the scatter diagram of $T_{\rm P}^{(\rm f)}$ as a function of $\lg E_0^{(\rm f)}$. $T_{\rm P}^{(\rm f)}$ was almost constant for $E_0^{(\rm f)}\leqslant 10^{-5}$. For $E_0^{(\rm f)}>10^{-5}$, $T_{\rm P}^{(\rm f)}$ shows a slow, almost linear decrease with increasing $\lg E_0^{(\rm f)}$. The regression between $T_{\rm P}^{(\rm f)}$ and $E_0^{(\rm f)}$ using Eq. (6) yields

$$\begin{cases} T_{\rm P}^{(\rm f)} = 7.35, \text{ if } E_0^{(\rm f)} \leqslant 10^{-5}\,, \\ T_{\rm P}^{(\rm f)} = -\dfrac{c}{11.0}\lg\dfrac{E_0^{(\rm f)}}{E_\infty^{(\rm f)}-E_0^{(\rm f)}} + 5.96\,, \\ \qquad \text{if } 10^{-5} < E_0^{(\rm f)} < E_\infty^{(\rm f)} \end{cases} \qquad (12)$$

where c=2.303 and $E_\infty^{(\rm f)}$=23.53. The fitting curve using Eq. (12) is shown in Fig. 12. According to Eq. (12), if the slow dynamics had a fixed initial error with magnitude equal to 10^{-5}, the predictability of the fast dynamics was limited to ∼7.35. For $E_0^{(\rm f)}>10^{-5}$, $T_{\rm P}^{(\rm f)}$ decreased with $\lg E_0^{(\rm f)}$ at a rate close to $c/\lambda_1^{(\rm f)}$.

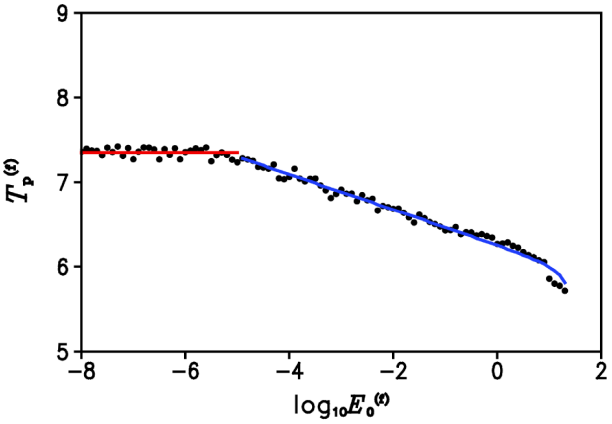

Fig. 12. Scatter diagram of the predictability limit of the fast dynamics $T_{\rm P}^{(\rm f)}$ versus $\lg E_0^{(\rm f)}$ in the coupled Lorenz model with $E_0^{(\rm s)} = 10^{-5}$. The red and blue lines are the curves fit by regression of the data shown by the solid circles using Eq. (12) for $E_0^{(\rm f)} \leqslant 10^{-5}$ and $10^{-5} < E_0^{(\rm f)} < E_\infty^{(\rm f)}$, respectively.

4. Conclusion

In this study, we determined the limits of predictability (defined here as the time at which the error reached 95% of its saturation level) for initial error of various magnitudes in the Lorenz model (Lorenz, 1963) and the coupled Lorenz model (Boffetta et al., 1998). Then we analyzed the relationship between the limit of predictability and initial errors in the Lorenz model and the coupled Lorenz model. We showed that a logarithmic function derived from the error growth model introduced by Lorenz (1982) performed well in describing the relationship between the limit of predictability and initial error in these two systems, although the coefficients in the logarithmic function were not constant across the examined range of initial errors. Compared with the Lorenz model, the coupled Lorenz model (in which the slow dynamics and the fast dynamics interact with each other) exhibited a more complex relationship between the limit of predictability and initial error.

In the Lorenz model, $T_{\rm p}$ decreased approximately linearly with increasing $\lg E_0$ for $E_0 < 10^{0.2}$ (where $10^{0.2}$ corresponds to the error above which the tangent linear approximation of error growth is no longer valid), while it decreased more quickly than linearly with increasing $\lg E_0$ for $E_0 \geqslant 10^{0.2}$. The logarithmic regression between $T_{\rm p}$ and E_0 shows that the maximal Lyapunov exponent λ_1 was relevant to the rate of change in $T_{\rm p}$ relative to E_0 for $E_0 < 10^{0.2}$ but not for $E_0 \geqslant 10^{0.2}$. This regression analysis also demonstrates that $T_{\rm P}$ was unbounded as E_0 approached 0. Therefore, the predictability limit of the Lorenz model can be extended as long as the initial error can be reduced.

In the coupled Lorenz model, the coupled fast dynamics dominated the average error growth during the initial stage for sufficiently small $E_0^{(\rm f)}$ and $E_0^{(\rm s)}$, while the coupled slow dynamics tended to dominate the average error growth at large $E_0^{(\rm f)}$ and $E_0^{(\rm s)}$. As a result, the predictability limit $T_{\rm P}^{(\rm f)}$ of the coupled fast dynamics was significantly extended for $E_0^{(\rm f)}$ of various magnitudes compared with that of the uncoupled fast dynamics. By contrast, the predictability limit $T_{\rm P}^{(\rm s)}$ of the coupled slow dynamics was significantly decreased for sufficiently small $E_0^{(\rm s)}$, but it was not evidently different from that of the uncoupled slow dynamics for relatively large $E_0^{(\rm s)}$. If the magnitudes of $E_0^{(\rm f)}$ and $E_0^{(\rm s)}$ both became infinitesimally small, $T_{\rm P}^{(\rm s)}$ and $T_{\rm P}^{(\rm f)}$ would be unbounded. However, if the fast dynamics has a fixed $E_0^{(\rm f)}$ (> 0), the slow dynamics has an intrinsic finite limit of predictability that cannot be extended by reducing the amplitude of $E_0^{(\rm s)}$, and vice versa.

Our results suggest that the limit of predictability of any coupled system that possesses many scales of time or motion is theoretically unbounded as long as the initial error can be continuously reduced. In reality, however, errors with finite magnitude are inevitable in the initial conditions of a geophysical system because of the limitations of observational instruments, thereby leading to an intrinsic finite limit of predictability in the system. Nevertheless, further study is required to examine how the predictability limit of a geophysical system that possesses many (i.e., more than two) scales of motion varies according to the initial error. It can be expected that additional scales of time or motion would amplify the complexity of the relationship between the limit of predictability and initial error.

Acknowledgements. Funding for this research was provided jointly by the 973 Program (Grant No. 2010CB950400) and National Natural Science Foundation of China (Grant Nos. 40805022 and 40821092).

REFERENCES

Benettin, G., L. Galgani, A. Giorgilli, and J. M. Strelcyn, 1980: Lyapunov characteristics exponents for smooth dynamical systems and for Hamiltonian systems; a method for computing all of them. *Meccanica*, **15**, 9–20.

Boffetta, G., P. Giuliani, G. Paladin, and A. Vulpiani, 1998: An extension of the Lyapunov analysis for the predictability problem. *J. Atmos. Sci.*, **55**, 3409–3416.

Chen, W. Y., 1989: Estimate of dynamical predictability from NMC DERF experiments. *Mon. Wea. Rev.*, **117**, 1227–1236.

Chou, J. F., 1989: Predictability of the atmosphere. *Adv. Atmos. Sci.*, **6**, 335–346.

Dalcher, A., and E. Kalnay, 1987: Error growth and predictability in operational ECMWF forecasts. *Tellus* A, **39**, 474–491.

Ding, R. Q., and J. P. Li, 2007: Nonlinear finite-time Lyapunov exponent and predictability. *Physics Letters A*, **364**, 396-400.

Ding, R. Q., G. L. Feng, S. D. Liu, S. K. Liu, S. X. Huang, and Z. T. Fu, 2006: Review of the study of nonlinear atmospheric dynamics in China (2003–2006). *Adv. Atmos. Sci.*, **24**, 1077–1085, doi: 10.1007/s00376-007-1077-7.

Eckmann, J. P., and D. Ruelle, 1985: Ergodic theory of chaos and strange attractors. *Reviews of Modern Physics*, **57**, 617–656.

Krishnamurthy, V., 1993: A predictability study of Lorenz's 28-variable model as a dynamical system. *J. Atmos. Sci.*, **50**, 2215-2229.

Leith, C. E., 1971: Atmospheric predictability and two-dimensional turbulence. *J. Atmos. Sci.*, **28**, 145–161.

Leith, C. E., and R. H. Kraichnan, 1972: Predictability of turbulent flows. *J. Atmos. Sci.*, **29**, 1041–1052.

Li, J. P., and R. Q. Ding, 2011a: Temporal–spatial distribution of atmospheric predictability limit by local dynamical analogues. *Mon. Wea. Rev.*, **139**, 3265–3283.

Li, J. P., and R. Q. Ding, 2011b: Relationship between the predictability limit and initial error in chaotic systems. *Chaotic Systems*, Esteban Tlelo-Cuautle, Ed., InTech Press, 39–50.

Lorenz, E. N., 1963: Deterministic nonperiodic flow. *J. Atmos. Sci.*, **20**, 130–141.

Lorenz, E. N., 1965: A study of the predictability of a 28-variable atmospheric model. *Tellus*, **3**, 321–333.

Lorenz, E. N., 1969a: The predictability of a flow which possesses many scales of motion. *Tellus*, **21**, 289–307.

Lorenz, E. N., 1969b: Atmospheric predictability as revealed by naturally occurring analogues. *J. Atmos. Sci.*, **26**, 636-646.

Lorenz, E. N., 1982: Atmospheric predictability experiments with a large numerical model. *Tellus*, **34**, 505–513.

Lorenz, E. N., 1996: Predictability: A problem partly solved. *Proc. ECMWF Seminar on Predictability*, Vol. I, Reading, United Kingdom, ECMWF, 1–18.

Metais, O., and M. Lesieur, 1986: Statistical predictability of decaying turbulence. *J. Atmos. Sci.*, **43**, 857–870.

Mu, M., W. S. Duan, and J. C. Wang, 2002: The predictability problems in numerical weather and climate prediction. *Adv. Atmos. Sci.*, **19**, 191–204.

Nohara, D., and H. L. Tanaka, 2001: Logarithmic relation between the initial error and predictability for the barotropic component of the atmosphere. *J. Meteor. Soc. Japan*, **79**, 161–171.

Oseledec, V. I., 1968: A multiplicative ergodic theorem: Lyapunov characteristic numbers for dynamical systems. *Trans. Moscow Math. Soc.*, **19**, 197–231.

Palmer, T. N., 2006: Predictability of weather and climate: From theory to practice. *Predictability of Weather and Climate*, T. Palmer and R. Hagedorn, Eds., Cambridge University Press, 1–10.

Shimada, I., and T. Nagashima, 1979: A numerical approach to ergodic problem of dissipative dynamical systems. *Progress of Theoretical Physics*, **61**, 1605–1616.

Simmons, A. J., R. Mureau, and T. Petroliagis, 1995: Error growth and estimates of predictability from the ECMWF forecasting system. *Quart. J. Roy. Meteor. Soc.*, **121**, 1739–1771.

Store, R., and J. F. Royer, 1993: Comparison of different error growth formulas and predictability estimation in numerical extended-range forecasts. *Ann. Geophys.*, **11**, 296–316.

Toth, Z., 1991: Estimation of atmospheric predictability by circulation analogs. *Mon. Wea. Rev.*, **119**, 65–72.

van den Dool, H. M., 1994: Searching for analogues, how long must we wait? *Tellus*, **46A**, 314–324.

Wolf, A., J. B. Swift, H. L. Swinney, and J. A. Vastano, 1985: Determining Lyapunov exponents from a time series. *Physica D*, **16**, 285-317.

Zhou, X. J., 2005: Atmospheric stochastic dynamics and predictability. *Acta Meteorologica Sinica*, **63**, 806–811. (in Chinese)